Impact of Silica Nanoparticle Design on Cellular Toxicity and Hemolytic Activity

Tian Yu,[†,§] Alexander Malugin,[†,§] and Hamidreza Ghandehari[†,‡,§,*]

[†]Department of Pharmaceutics and Pharmaceutical Chemistry, [‡]Department of Bioengineering, and [§]Utah Center for Nanomedicine, Nano Institute of Utah, University of Utah, Salt Lake City, Utah, 84108, United States

ABSTRACT Understanding the toxicity of silica nanoparticles (SiO_2) on the cellular level is crucial for rational design of these nanomaterials for biomedical applications. Herein, we explore the impacts of geometry, porosity, and surface charge of SiO_2 on cellular toxicity and hemolytic activity. Nonporous Stöber silica nanospheres (115 nm diameter), mesoporous silica nanospheres (120 nm diameter, aspect ratio 1), mesoporous silica nanorods with aspect ratio of 2, 4, and 8 (width by length 80 × 200 nm, 150 × 600 nm, 130 × 1000 nm), and their cationic counterparts were evaluated on macrophages, lung carcinoma cells, and human erythrocytes. It was shown that the toxicity of SiO_2 is cell-type dependent and that surface charge and pore size govern cellular toxicity. Using inductively coupled plasma mass spectrometry, the cellular association of SiO_2 was quantitated with the association amount increasing in the following order: mesoporous SiO_2 (aspect ratio 1, 2, 4, 8) < amine-modified mesoporous SiO_2 (aspect ratio 1, 2, 4, 8) < amine-modified nonporous Stöber SiO_2 < nonporous Stöber SiO_2. Geometry did not seem to influence the extent of SiO_2 association at early or extended time points. The level of cellular association of the nanoparticles was directly linked to the extent of plasma membrane damage, suggesting a biological cause-and-effect relationship. Hemolysis assay showed that the hemolytic activity was porosity- and geometry-dependent for bare SiO_2 and surface-charge-dependent for amine-modified SiO_2. A good correlation between hemolytic activity and cellular association was found on a similar dosage basis. These results can provide useful guidelines for the rational design of SiO_2 in nanomedicine.

KEYWORDS: silica · nanotoxicity · nanomedicine · silica nanorods · porous SiO_2

Silica-based nanomaterials have attracted much attention in biomedical applications as cell markers, gene transfection agents, imaging moieties, and drug carriers.[1−5] They possess a variety of unique properties, such as ease of synthesis, availability of surface modification, robust mechanical properties, and relatively inert chemical composition.[6,7] Synthetic strategies in template fabrication have further enabled the production of silica nanomaterials with distinct shape features, with increasing interest in their evaluation in biological systems.[8−11] Despite these advantages, the influence of physicochemical factors such as geometry, pore size, and surface functional groups of SiO_2 still needs to be carefully examined for successful utility of these constructs in nanomedicine.[12]

Emerging literature suggests that nano- and microparticle shape can influence cellular uptake and biodistribution.[13−15] For example it has been reported that high-aspect-ratio cationic hydrogel particles (150 × 450 nm) were internalized by HeLa cells four times faster than corresponding low-aspect-ratio particles (200 × 200 nm).[13] Other reports suggest that uniform micrometer-sized polystyrene beads with elliptical disk shape had a longer half-life in circulation than their spherical counterparts and less residence time in the liver.[14] We have previously demonstrated that PEGylated gold nanorods (10 × 45 nm, 1.13 mV) had less liver uptake, longer blood circulation half-life, and higher tumor accumulation than PEGylated gold nanospheres (50 nm, −27.1 mV) in orthotopic ovarian tumor xenograft mice.[15] In addition to geometry, porosity and surface functionality of nanoparticles are also critical factors that can influence the interaction of silica nanoparticles with biological systems.[16−18] The pore size of SiO_2 is a key factor in determining the adsorption capacity of proteins such as bovine serum albumin, where the adsorption capacity was elevated as the pore size of SiO_2 increased.[16] Maurer-Jones *et al.* have demonstrated that 25 nm, nonporous SiO_2 had a greater impact on cells than 25 nm porous SiO_2 since the former possessed higher "cell-contactable reactive surface area" to perturb cell function.[17] Slowing *et al.* have reported that the uptake of mesoporous silica nanoparticles by cervical cancer cells could be elevated by surface functionalization with cationic functionalities or targeting moiety.[18] Despite these initial studies, there is a need for a systematic investigation of the interdependent roles of nanoparticle geometrical effect, porosity, and surface functionality on cellular uptake

* Address correspondence to hamid.ghandehari@pharm.utah.edu.

Received for review April 15, 2011 and accepted June 1, 2011.

Published online June 01, 2011
10.1021/nn2013904

TABLE 1. Synthetic Conditions of Nonporous and Mesoporous SiO_2 and Their Physical Characterization of Size, Surface Area, and Pore Size[a]

	composition (CTAB:H_2O:NH_4OH: TEOS)	stirring rate (rpm)	temp (°C)	size by TEM (nm)	aspect ratio	surface area (m^2/g)	external surface area (m^2/g)	pore volume (cm^3/g)	pore size (nm)
Stöber	see "Methods"	550	40	115 ± 13	1.0	24[b]	24[b]	N/A	N/A
Meso S	0.1:1000:7:0.7	250	22	120 ± 25	1.0	663	109	0.63	2.7
AR2	0.2:1000:5:0.7	230	22	77 ± 9 × 198 ± 53	2.5	443	102	0.59	2.7
AR4	0.4:1000:10:1.4	350	22	159 ± 49 × 594 ± 82	3.8	1191	231	1.17	2.8
AR8	0.4:1000:10:1.4	250	22	136 ± 26 × 1028 ± 139	7.6	284	47	0.26	2.7

[a] Data are mean ± SD ($n = 3$). [b] Based on theoretical calculation as shown in Supplemental Calculation 1.

and toxicity.[19−21] Such studies will enable the elucidation of predominant factors that determine the extent of toxicity, which will then provide practical guidance for rationally designing SiO_2 as biomedical devices with minimum adverse effects.

In this study, multiple physicochemical parameters of SiO_2 were evaluated for their effects on cellular toxicity and hemolytic activity. In order to compare the effect of pore size, mesoporous and nonporous spherical SiO_2 of the same diameter (*ca.* 110 nm) were synthesized and evaluated. To demonstrate the effect of geometrical feature (represented as aspect ratio, ratio of length over width), silica nanorods were produced with similar diameters along the short axis (around 100 nm) and different lengths along the long axis (approximately 200, 600, and 1000 nm). SiO_2 of different porosities and aspect ratios were modified with primary amine silane groups to generate cationic charge, which is dramatically different from the anionic charge of bare silica nanoparticle counterparts, to assess the impact of surface charge. SiO_2 with the engineered physicochemical features as mentioned above were subject to a series of toxicity assays on two model cell lines, namely, RAW 264.7 (a model macrophage commonly used to represent the physiological scavengers of foreign nanoparticles exposed to *in vivo* systems[22]) and A549 (non-small-cell lung cancer epithelial cells). These cells were selected as model cells for potential targeted delivery of bioactive and imaging agents. We further characterized the hemolytic activity of SiO_2 as an initial step to evaluate *ex vivo* blood biocompatibility.

RESULTS AND DISCUSSION

Nanoparticle Synthesis and Characterization. Nonporous SiO_2[23] and mesoporous SiO_2 of different geometrical features were synthesized and characterized using transmission electron microscopy (TEM), X-ray diffraction (XRD), and nitrogen adsorption−desorption analysis for size, mesopore arrangement, surface area, and pore size measurement (Table 1). Mesoporous SiO_2 of different shapes were synthesized by a one-step condensation and aging method.[19,24−29] In the first step, mesoporous SiO_2 was formed by condensation under dilute silica source and low surfactant concentration conditions with ammonium hydroxide as the base catalyst. The shape and polydispersity of SiO_2 were mainly controlled by molar composition of reaction agents[24−28] and stirring rate.[29] By changing the concentration of tetraethyl orthosilicate (TEOS), cetyltrimethylammonium bromide (CTAB), and aqueous ammonia and reaction stirring rate, mesoporous SiO_2 with targeted diameters (*ca.* 100 nm), lengths, and aspect ratios (1, 2, 4, 8) were synthesized. In general, the width of mesoporous SiO_2 was controlled by adjusting the ammonia concentration in the reaction mixture,[19] with larger width obtained at increased ammonia concentration, while the length of mesoporous SiO_2 increased with increased TEOS concentration, increased CTAB concentration, increased ammonia concentration, and reduced stirring speed.[28,29] In the second step, mesoporous silica nanoparticles were subject to autoclaving at 100 °C for 24 h to promote silica matrix cross-linking and to enhance the stability of mesopore structure.[30,31]

Evident from TEM image analysis (Figure 1), nonporous silica nanospheres (Stöber) and mesoporous silica nanospheres (Meso S) were 115 ± 13 and 120 ± 25 nm in diameter, respectively. Mesoporous silica nanorods were produced with distinctly different geometrical features. They possessed similar diameter to that of nanospheres (around 100 nm), yet the aspect ratios were different (mesoporous SiO_2 with aspect ratios 2, 4, and 8 are abbreviated as AR2, AR4, and AR8, respectively). The aspect ratio distribution histogram showed that each type of mesoporous SiO_2 possessed distinct shape characteristics compared with any other type of mesoporous SiO_2 (Figure 1G), except AR2 and AR4 had a certain portion of overlapped aspect ratios. However, they still possessed distinct geometrical features considering their dimensions were significantly different from each other along the short or long axes.

Figure 2A−D presents the nitrogen adsorption−desorption isotherms for mesoporous SiO_2 of different shapes. Mesoporous SiO_2 exhibited type IV isotherms, which were typical of a mesopore structure. The filling of mesopores occurred at relative pressure (P/P_0) of 0.3

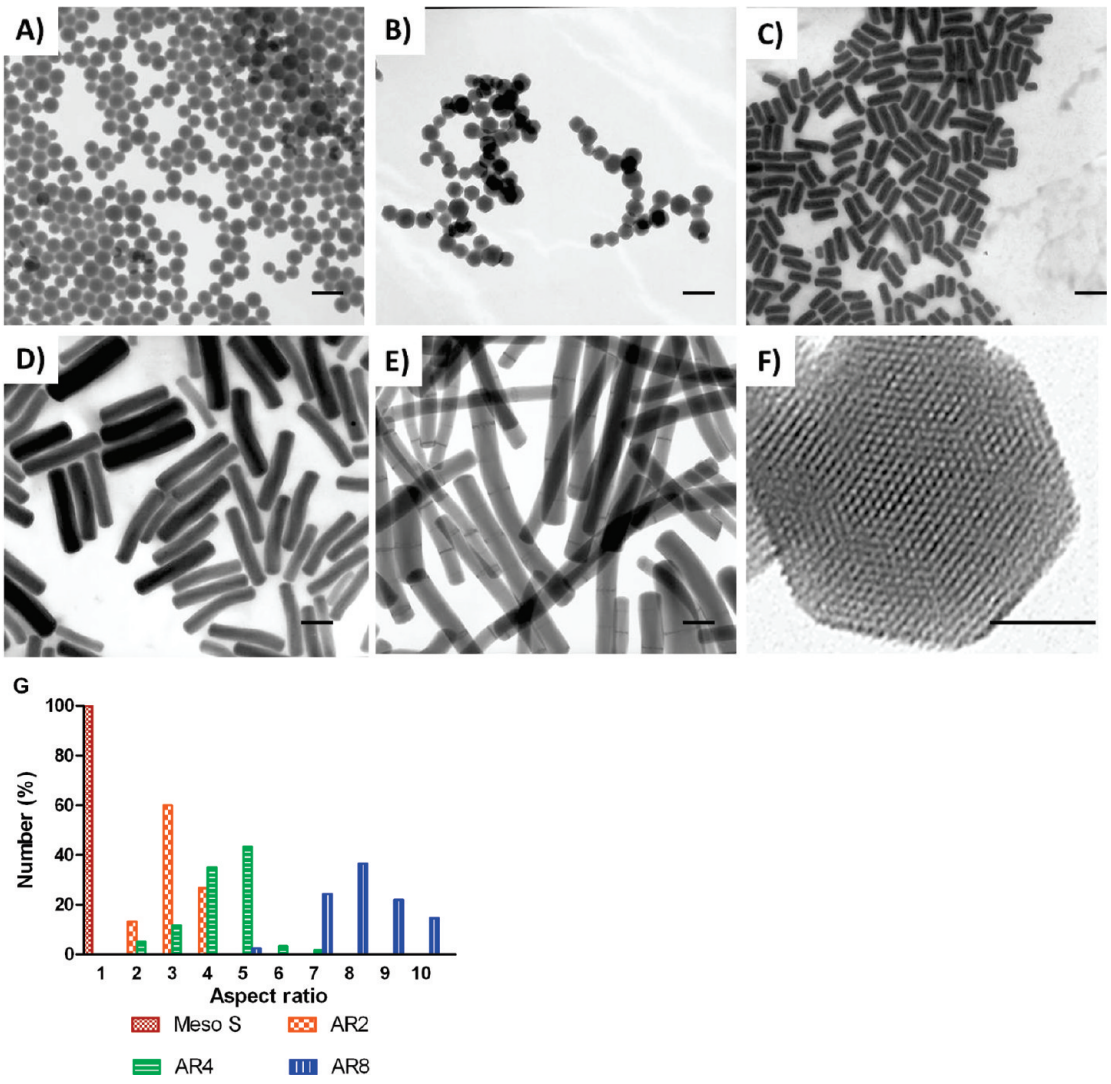

Figure 1. Transmission electron microscopy images of (A) Stöber SiO_2 with average diameter of 115 nm (referred to as Stöber), (B) mesoporous SiO_2 with average diameter of 120 nm (Meso S), (C) mesoporous silica nanorods with aspect ratio 2 (AR2), (D) mesoporous silica nanorods with aspect ratio 4 (AR4), (E) mesoporous silica nanorods with aspect ratio 8 (AR8), and (F) high-resolution image of a single particle in B. (G) Percentage distribution histogram as a function of aspect ratio. Scale bars in A–E = 200 nm, scale bar in F = 50 nm.

to 0.5. Each type of nanoparticles also exhibited an additional capillary condensation at high relative pressure ($P/P_0 > 0.90$), which was characteristic of a high degree of textural porosity.[19,21] Mesoporous SiO_2 possessed relatively high surface area (280–1190 m^2/g) as calculated by the Brunauer–Emmet–Teller method (Table 1).[19,21] The external surface areas of mesoporous SiO_2, which referred to cell-contactable surface area, were calculated from the *t* plots of their N_2 adsorption isotherms (Table 1).[32] Different mesoporous nanoparticles displayed a narrow distribution of pore size, which centered around 2.7–2.8 nm in diameter, as determined by the Barrett–Joyner–Halenda method (Table 1).[19,21] Meso S possessed typical MCM-41 type mesopore arrangement, as reflected by the distinct peaks (100, 110, 200, 210) in the XRD measurement (Figure 2E), which was in good agreement with its high-resolution TEM image (Figure 1F), showing 2D-hexagonal mesopores in the close-packing structure for this type of SiO_2.[28] The mesopore structure of Meso S was also well maintained post amine modification (Figure 2F). Therefore, Meso S was compared with nonporous Stöber nanoparticles to study the pore size effect on cellular toxicity and hemolytic activity.

The dynamic light scattering measurements showed that the Meso S tended to agglomerate to a higher extent (257.8 ± 0.9 nm) and was thus more polydisperse in size distribution than nonporous Stöber nanoparticles (148.0 ± 0.4 nm) (Table 2). Due to the method limitations, dynamic light scattering measurements are not applicable to the mesoporous silica nanorod structure because this measurement model assumes a spherical shape of nanoparticles in suspension.[29] Zeta potential measurements showed that Stöber nanoparticles were highly negatively charged (−50.4 ± 1.0 mV), indicating a fairly stable suspension

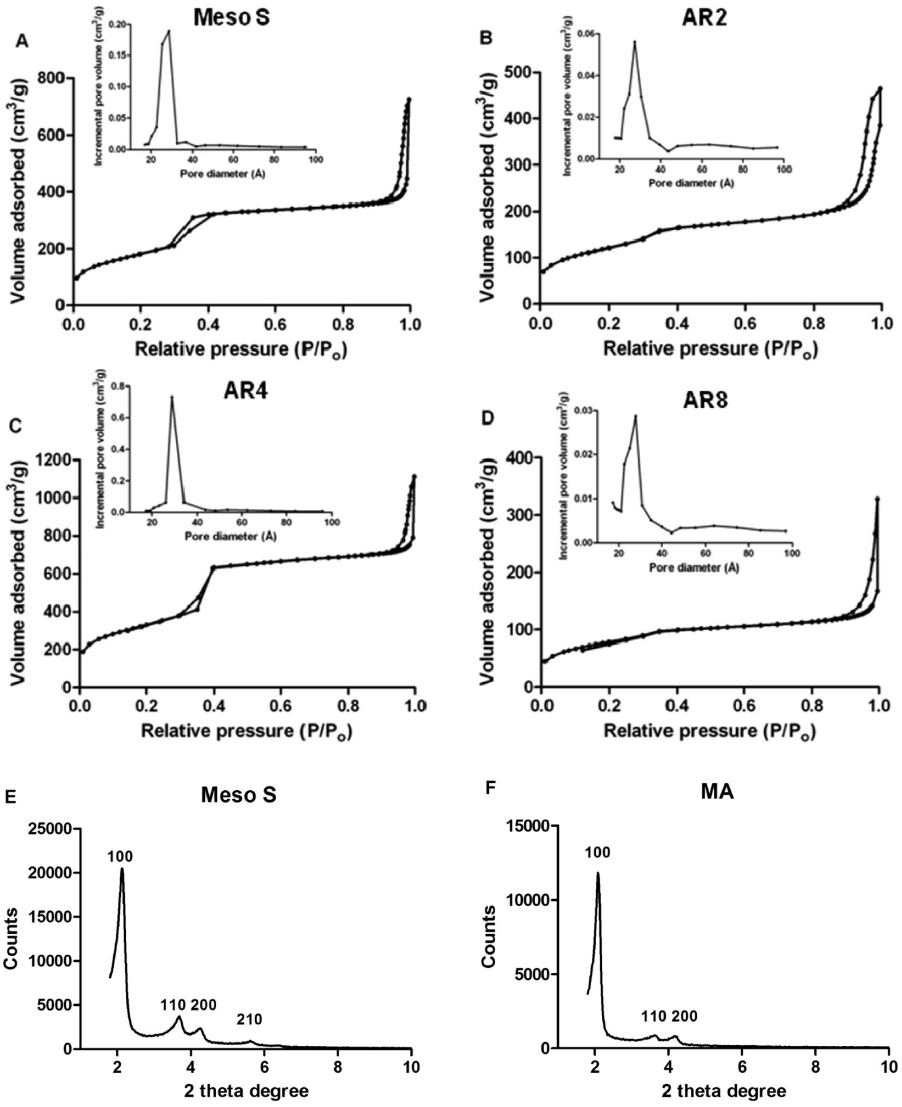

Figure 2. Nitrogen adsorption−desorption isotherms of (A) Meso S, (B) AR2, (C) AR4, and (D) AR8 mesoporous SiO_2. Insets are pore size distribution plots for each type of SiO_2. X-ray diffraction patterns of (E) Meso S and (F) MA. Both Meso S and MA exhibited the typical diffraction patterns of MCM-41 type mesoporous SiO_2 with hexagonal symmetry. The reduction in intensity of the MA diffraction pattern and the missing 210 peak might be due to the pore-filling effects caused by silane modification.[21]

TABLE 2. Hydrodynamic Size and Surface Charge of SiO_2 before and after Primary Amine Modification in Aqueous Suspension at pH 7.0[a]

	before APTES modification		post APTES modification	
	size by DLS (nm)/PDI	zeta potential (mV)	size by DLS (nm)/PDI	zeta potential (mV)
Stöber	148.0 ± 0.4/0.043	−50.4 ± 1.0	174.2 ± 1.9/0.102	17.0 ± 0.7
Meso S	257.8 ± 0.9/0.219	−39.4 ± 0.5	233.8 ± 2.2/0.145	32.4 ± 0.9
AR2	N/A	−33.5 ± 0.5	N/A	32.0 ± 1.0
AR4	N/A	−34.0 ± 1.2	N/A	40.3 ± 1.0
AR8	N/A	−36.6 ± 0.6	N/A	36.7 ± 0.5

[a] Data are mean ± SD (n = 3).

in aqueous medium.[33] Amine-modified Stöber (SA) nanoparticles had a relatively lower positive zeta potential (17.0 ± 0.7 mV), which implied a moderate stability in aqueous suspension (Table 2).[31] Mesoporous SiO_2 was highly negatively charged (<−30 mV) as bare nanoparticles and was highly positively charged (>30 mV) post amine modification, which indicated a high stability within suspension (the amine-modified mesoporous nanospheres or nanorods with aspect ratios of 2, 4, and 8 are abbreviated as MA, 2A, 4A, and 8A).[33] The absence of a carbon chain band (wavenumber 3000−2800) in the FT-IR spectrum of surfactant-removed nanoparticles confirmed the complete removal of CTAB from the products by the acidic ethanol extraction method (Supplemental Figure 1). The end point chromogenic Limulus Amebocyte Lysate (LAL) test (Lonza, Walkersville, MD) showed that there was no detectable Gram-negative endotoxin on any type of nanoparticles at 1 mg/mL (the detection

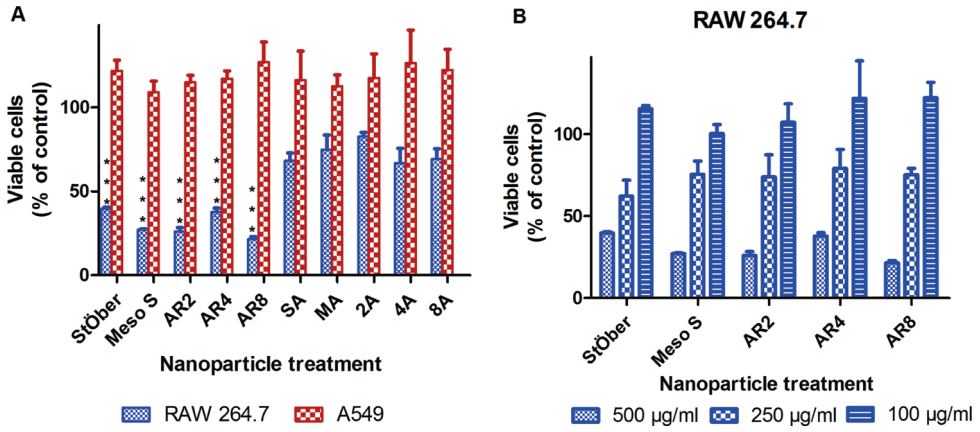

Figure 3. (A) Acute cytotoxicity assay of indicated cells incubated with bare and amine-modified SiO_2 at 500 μg/mL. (B) Acute cytotoxicity assay of RAW 264.7 cells after incubating with bare SiO_2 at 500, 250, and 100 μg/mL for 24 h. ***Relative viability of bare silica nanoparticle-treated cells was significantly lower than that of amine-modified counterpart-treated cells ($p < 0.001$). Data are mean $\pm$ SD ($n = 3$).

limit was less than 0.1 EU/mL), which was the highest concentration of nanoparticles used in the *in vitro* and *ex vivo* studies.

Acute Cytotoxicity. The ability of SiO_2 with the engineered physicochemical features to induce acute cellular toxicity response was tested on RAW 264.7 and A549 cells by WST-8 assay. Results demonstrated that toxicity of SiO_2 was highly cell-type- and nanoparticle-concentration-dependent (Figure 3). All types of SiO_2 at concentrations as high as 500 μg/mL did not affect the relative viability of A549 cells after 24 h exposure. For RAW 264.7 macrophages, nonporous or mesoporous SiO_2 caused dramatic toxicity post 24 h incubation, leaving only *ca.* 20−40% viable cells compared with controls, while amine-modified counterparts caused limited toxicity with approximately 64−85% relative viability (Figure 3A). Since bare SiO_2 showed higher cytotoxicity on RAW 264.7, doses that led to reduced toxicity (250 μg/mL with *ca.* 70% viability) or nontoxicity (100 μg/mL with *ca.* 100% viability) have been identified (Figure 3B) to be used in the following plasma membrane integrity assay or nanoparticle cellular association quantitation assay.

Proliferation Inhibition. The ability of nanoparticles to inhibit cell proliferation was cell-type-dependent (Figure 4). Cancer epithelial cells were resistant to all types of nanoparticle treatment up to 500 μg/mL post 72 h exposure, and only cells treated with 2A and 8A at 1000 μg/mL exhibited a moderate toxicity response, resulting in 60−70% viable cells compared with controls (Figure 4A,B). For macrophages, the nanoparticle concentration that led to 50% inhibition on cell growth (IC_{50}) ranged approximately from 50 to 100 μg/mL post 3-day exposure for bare SiO_2 (Figure 4C), and the IC_{50} values of bare nonporous and mesoporous SiO_2 were not distinguishable from one another ($p > 0.05$). Interestingly, the reduction of IC_{50} was not observed for nanoparticles post amine modification. Instead, a several fold increase in IC_{50} was detected for amine-modified nanoparticles (Figure 4D, Table 3). For example, the IC_{50} values of AR4 and 4A were 91.6 $\pm$ 5.9 and 184.2 $\pm$ 17.1 μg/mL, respectively, and the IC_{50} values of AR8 and 8A were 73.7 $\pm$ 17.0 and 224.9 $\pm$ 28.2 μg/mL, respectively. Changes in cell morphology were observed in RAW 264.7 post nanoparticle exposure for 24 h (Supplemental Figure 2) or 72 h (Supplemental Figure 3). Reduced cell density and rounded cells were observed for bare SiO_2 treated macrophages, while swollen vacuoles in cells were frequently observed in amine-modified SiO_2 treated macrophages.

To assess whether toxicity was due to soluble factors that were released from nanoparticles,[12] the toxicity assay was performed on the supernatant of nanoparticle stock aqueous suspension. Results showed that the supernatant did not affect the relative viability compared with controls (data not shown). To evaluate whether toxicity was due to adsorbed endotoxin on nanoparticles[34] that was below the detection limit of the LAL assay (<0.1 EU/mL), endotoxin from reference standard *E. coli* stock was added to make 0.1 EU/mL concentration in the 500 μg/mL nanoparticle suspension. Results showed that the relative viability post 24 h incubation and IC_{50} of nanoparticles post 72 h exposure were not changed in the presence of added endotoxin compared with nanoparticle treatment without addition of endotoxin (data not shown). These results support the fact that the toxicity of SiO_2 was due to cellular interaction with nanoparticles themselves, rather than a product of degradation or any associated contaminants. In order to look into the cause for reduced toxicity of amine-modified SiO_2, we conducted inductively coupled plasma mass spectrometry (ICP-MS) analysis on cells treated with nanoparticles, and the results are discussed in Cellular Association section.

Plasma Membrane Integrity. Plasma membrane damage is an important aspect of cellular toxicity upon nanoparticle treatment. When cells have plasma membrane damage, the propidium iodide in the solution

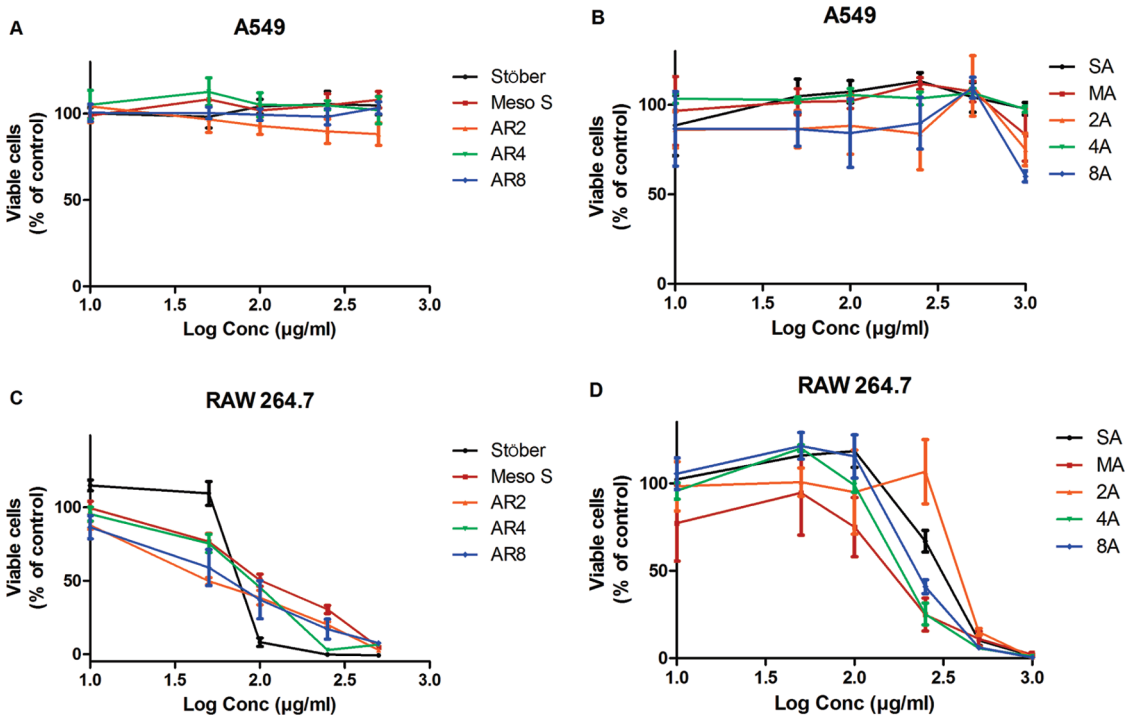

Figure 4. Proliferation inhibition assay of A549 (A, B) and RAW 264.7 (C, D) cells after continuous 72 h incubation with bare (A, C) and amine-modified (B, D) SiO_2. Data are mean ± SD (n = 3).

TABLE 3. Summary of IC_{50} Values of SiO_2 on RAW 264.7 Macrophages[a]

	IC_{50} values (μg/mL)				
	Stöber	Meso S	AR2	AR4	AR8
bare nanoparticles[b]	73 ± 3	89 ± 4	72 ± 12	92 ± 6	74 ± 18
amine-modified nanoparticles	254 ± 15	182 ± 38	471 ± 7	184 ± 17	225 ± 28

[a] Data are mean ± SD (n = 3). [b] There was no significant difference in IC_{50} among all types of bare SiO_2 ($p > 0.05$); however, statistically significant differences were observed between IC_{50}'s of each type of bare SiO_2 and that of their amine-modified counterparts ($p < 0.001$).

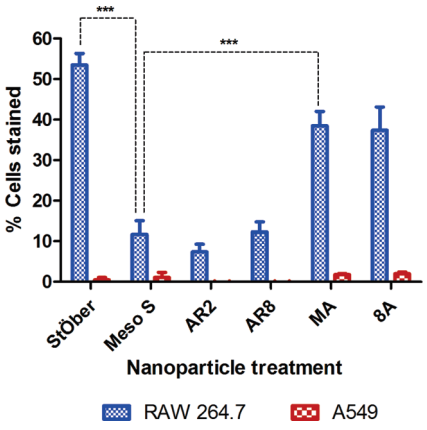

Figure 5. Percentage of propidium iodide stained cells in RAW 264.7 cells (blue bars) or A549 cells (red bars) after incubating with 250 μg/mL SiO_2 for 24 h. ***Meso S led to significantly decreased percentage of propidium iodide positive cells compared with Stöber or MA ($p < 0.001$). Data are mean ± SD (n = 3).

passively diffuses into the cytoplasm and binds with intracellular DNA or RNA. By quantitating the percentage of propidium iodide positive cells, one could deduct the percentage of cells experiencing plasma membrane damage in the total cell population.[35] The results show that the ability of nanoparticles (250 μg/mL) to compromise the integrity of plasma membrane after 24 h incubation was cell-type-dependent (Figure 5). For cancer epithelial cells, the percentage of propidium iodide positive cells was less than 3% for all types of SiO_2 treatment. For macrophages, Stöber nanoparticles caused plasma membrane damage in 53% of the cell population, while all mesoporous SiO_2 selected for this study caused plasma membrane damage in 6–15% of the RAW 264.7 cell population. Stöber nanoparticles caused the highest percentage of propidium iodide positive cells probably due to their high silanol density on the external surface that was accessible to the cell membrane, which caused significantly higher cellular impact than mesoporous SiO_2.[36] Amine-modified mesoporous SiO_2 generated a higher extent of plasma membrane damage in *ca.* 38% of the cells than their bare mesoporous counterparts. Plasma membrane damage in cells was probably not due to the sedimentation of the nanoparticles, as this experiment was repeated with nanoparticles being added before cells were carefully plated on top of the nanoparticles, and the observed results were very similar (Supplemental Figure 4). Combining the results above, it

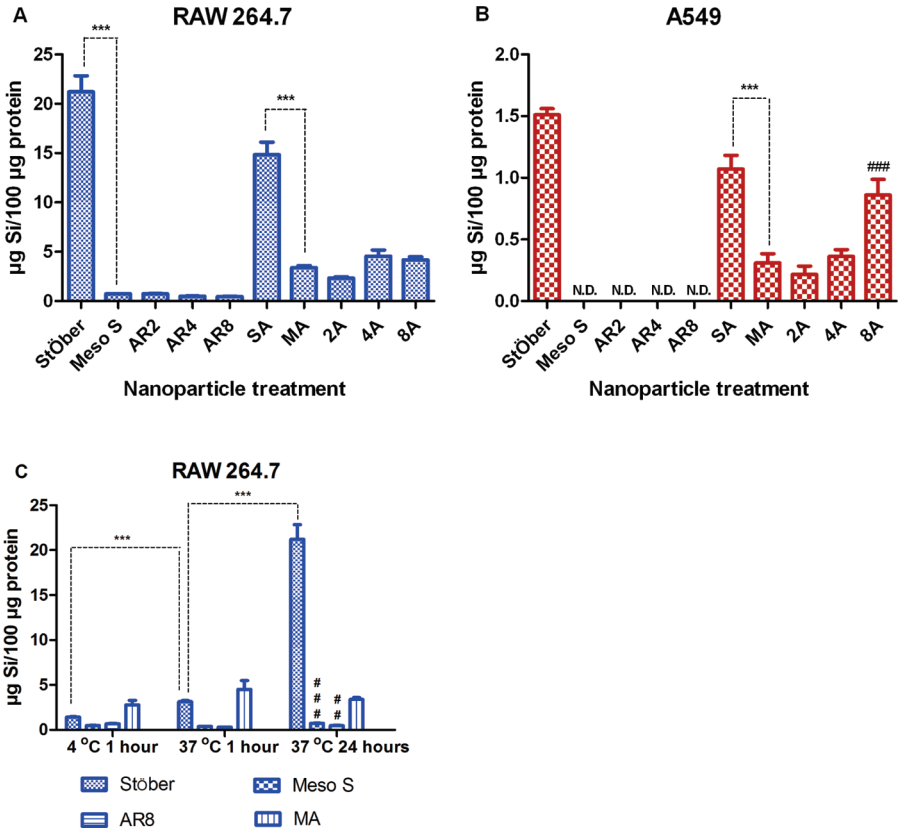

Figure 6. Inductively coupled plasma mass spectrometry (ICP-MS) analysis of cellular association of SiO_2 in (A) RAW 264.7 and (B) A549 cells post-incubation with nanoparticles at 100 μg/mL for 24 h. The graph shows the mass of silicon per 100 μg protein content *versus* different nanoparticle treatments. ***The level of cell-associated silicon was significantly higher in Stöber or SA-treated cells than in the mesoporous counterpart treated cells ($p < 0.001$). ###The level of cell-associated silicon was significantly higher in high aspect ratio, 8A-treated cells than in MA-, 2A-, or 4A-treated cells ($p < 0.001$). N.D. means "not detected". (C) Cellular association of SiO_2 after RAW 264.7 cells were incubated with 100 μg/mL selected SiO_2 at 4 °C (1 h) and 37 °C (1 or 24 h). The level of cellular-associated silicon was significantly higher at 24 h than at 1 h post-incubation with Stöber (*, $p < 0.001$), Meso S (###, $p < 0.001$), or AR8 (##, $p < 0.01$) at 37 °C. One-hour incubation with Stöber at 37 °C led to significantly higher silicon association than incubation at 4 °C (***, $p < 0.001$). Data are mean ± SD ($n = 3$).**

seems that porosity and surface charge are the major factors that determine the extent of plasma membrane damage in cells.

Cellular Association. The amount of cellular-associated SiO_2, which included internalized nanoparticles or nanoparticles adhering to the extracellular matrix, was quantitated by ICP-MS.[19] Results show a similar pattern of cellular association of SiO_2 with macrophages and cancer epithelial cells. However, the amount of silicon associated with macrophages was 10−15 times higher than that of the cancer epithelial cells (Figure 6A,B). Nonporous Stöber nanoparticles led to much higher cellular association than mesoporous nanoparticles both on a particle mass basis and on a particle number basis (Table 4). The level of cellular association was also highest for Stöber nanoparticles among all types of SiO_2 including the amine-modified counterparts SA. This observation was possibly due to the highest silanol density on the continuous external surface of Stöber nanoparticles, which was reflected by the highest magnitude of negative charge (−50 mV) for these particles.[36] The formation of porous structure or modification with primary amine groups led to reduced silanol density on the external surface of the particles (−33 to −39 mV for mesoporous SiO_2) or shielding of surface silanol by amine functionalities, which reduced the accessibility of silanol groups to cells and in turn decreased the level of cellular association.[36]

TABLE 4. Average Cellular Association of Bare SiO_2 Detected by ICP-MS on RAW 264.7 Post-incubating with Nanoparticles at 100 μg/mL for 24 h[a]

nanoparticle treatment	silicon content (μg)/100 μg protein	no. nanoparticles/ 100 μg protein
Stöber	21.2	2.6×10^{11}
Meso S	0.7	1.6×10^{10}
AR2	0.8	2.2×10^{10}
AR4	0.5	1.8×10^{9}
AR8	0.5	6.1×10^{8}

[a] There was no significant difference in the amount of cellular-associated silicon content per 100 μg of protein among various types of mesoporous SiO_2 ($p > 0.05$). Stöber nanoparticles were associated with RAW 264.7 at significantly higher levels than mesoporous SiO_2 of all types either in mass concentration or in number concentration ($p < 0.001$). Data are mean of triplicates.

On the other hand, amine-modified mesoporous SiO_2 (32−40 mV) showed significantly higher cellular association than their bare mesoprous counterparts ($p < 0.05$), which appeared to contradict the aforementioned phenomenon with SA (17 mV) and Stöber nanoparticles. This indicated that there could be a surface charge "threshold" (>30 mV) above which the amine functionalities facilitated nanoparticle−cell interaction through electrostatic interaction of positively charged amine groups with negatively charged cell membrane, whereas below the "threshold", there were less surface amine groups available and they had electrostatic interactions with surface silanols and covered the sites of silanol,[37] which eventually reduced the level of cellular association.

Bare mesoporous SiO_2, irrespective of their shape features, exhibited a similar level but the lowest amount of cellular-associated silicon. For A549 cells, the level of cell-associated silicon from mesoporous SiO_2 exposure was even below the detection limit of ICP-MS (<0.1 μg/mL for silicon element). There was no significant difference in the level of cellular association among all types of mesoporous SiO_2 ($p > 0.05$). There was also no significant difference in the cellular association among all mesoporous SiO_2 post amine modification on both cell lines ($p > 0.05$), except that 8A had a significantly higher cellular association than other amine-modified mesoporous SiO_2 on A549 cells ($p < 0.001$). This suggests that the curvature of cationic SiO_2 could influence the wrapping by the cell membrane and affect the cellular association with nonphagocytic cells.[13]

In order to test if porosity, geometry, and surface modification can influence the cellular association at earlier time points, selected SiO_2 including Stöber, Meso S, AR8, and MA were incubated with RAW 264.7 cells for 1 h, and the level of cellular association was detected by ICP-MS. The experiment was done at 4 or 37 °C to differentiate the amount of membrane-bound SiO_2 from that of internalized SiO_2, as incubation at low temperature (4 °C) drastically reduces the energy-dependent internalization process in cells.[38] Considering that the viability of cells could be affected upon incubation at 4 °C, which subsequently could influence the protein content recovered, the relative viability of cells post 70 min incubation (10 min preincubation and 60 min incubation with nanoparticles) at 4 °C was measured, and the results show that the percentage of viable cells was 94 ± 8% compared with control cells treated at 37 °C for the same time duration. As shown in Figure 6C, Stöber nanoparticles led to a significant increase in cellular association 24 h post-incubation at 37 °C compared with 1 h incubation at 37 °C ($p < 0.001$) or at 4 °C ($p < 0.001$), indicating that there was extenzsive internalization of nonporous nanoparticles over 24 h. There was no significant difference in cellular association between Meso S and AR8 post 1 h incubation at 37 °C ($p > 0.05$). Geometry did not seem to affect the level of cellular-associated nanoparticles for mesoporous SiO_2 at the early time points as well. Most mesoporous SiO_2 seemed to bind to the cell membrane instead of being internalized into the cytoplasm within an hour, as the level of silicon association from Meso S or AR8 exposure was similar for cells incubated at 4 or 37 °C for one hour. However, the level of cellular association significantly increased post-incubation for 24 h compared with incubation for 1 h at 37 °C for Meso S ($p < 0.001$) and AR8 ($p < 0.01$), which indicated that internalization of mesoporous SiO_2 had occurred. On the contrary, there was no significant difference in cellular association between 1 h incubation and 24 h incubation with MA at 37 °C ($p > 0.05$), which implied that the cellular association of MA almost reached a plateau within 1 h post-incubation. The cellular association of MA post 1 h incubation at 37 °C was not significantly higher than that at 4 °C ($p > 0.05$). The combined results suggest that there was limited internalization over 24 h post-incubation with MA, which probably explained why there was a reduction in toxicity of amine-modified SiO_2 compared with that of bare SiO_2. It has been suggested that the strong association of cationic SiO_2 with negatively charged cell membranes, which made the cationic SiO_2 adhere to the cell membrane instead of bringing them into the cytoplasm, led to the reduction in internalization and the resultant decreased toxicity based on transmission electron microscopy analysis[39−41] or confocal microscopy analysis.[42] Our results provide quantitative evidence by ICP-MS that there was limited internalization of amine-modified SiO_2.

In summary, it appears that surface charge and porosity mainly influenced the extent of cellular association, while geometry did not seem to influence cellular association within the aspect ratio range of 1−8 studied. These observations are consistent with the experiments examining plasma membrane integrity post nanoparticle treatment. The level of plasma membrane damage by nanoparticles was directly related to the extent of nanoparticle cellular association, which indicated a biological cause-and-effect relationship between cellular association and cell membrane damage on both cell lines.

Hemolysis. The impact of nanoparticle porosity, geometry, and surface functionality on human red blood cells (RBCs) was evaluated by a hemolysis assay. The quantitation of hemoglobin in the supernatant of a nanoparticle−RBC mixture was done by recording the absorbance of hemoglobin at 577 nm with a reference wavelength of 655 nm (Supplemental Figure 5).[36,43] Results show that the extent of hemolysis was concentration-, porosity-, and geometry-dependent for bare SiO_2 (Figure 7). Stöber nanoparticles caused an immediate onset of hemolysis that soon reached a plateau of 17% hemolysis at *ca.* 250 μg/mL probably

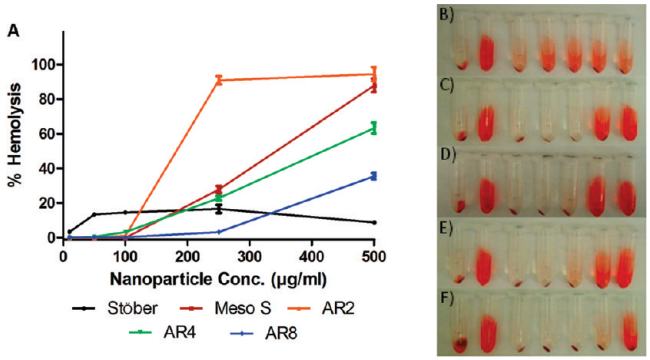

Figure 7. Hemolysis assay on bare SiO_2. (A) Relative rate of hemolysis in human RBCs upon incubation with nanoparticle suspension at incremental concentrations. The presence of hemoglobin in the supernatant (red) was observed in (B) Stöber suspension, (C) Meso S suspension, (D) AR2 suspension, (E) AR4 suspension, and (F) AR8 suspension. The tubes are lined up (from left to right) as negative control (PBS), positive control (water), 10 μg/mL suspension, 50 μg/mL suspension, 100 μg/mL suspension, 250 μg/mL suspension, and 500 μg/mL suspension. Data are mean ± SD (n = 3).

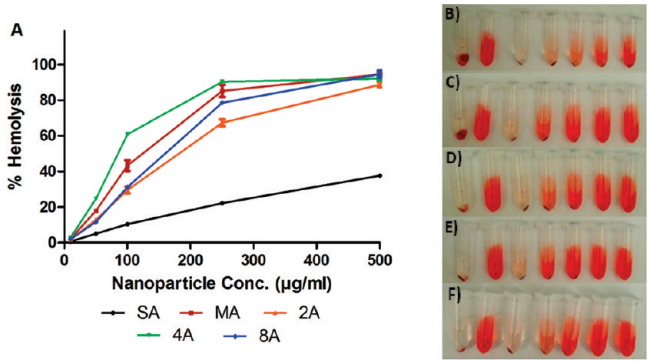

Figure 8. Hemolysis assay on amine-modified SiO_2. (A) Relative rate of hemolysis in human RBCs upon incubation with amine-modified nanoparticle suspension at incremental concentrations. The presence of hemoglobin in the supernatant (red) was observed in (B) SA suspension, (C) MA suspension, (D) 2A suspension, (E) 4A suspension, and (F) 8A suspension. The tubes are lined up (from left to right) as negative control (PBS), positive control (water), 10 μg/mL suspension, 50 μg/mL suspension, 100 μg/mL suspension, 250 μg/mL suspension, and 500 μg/mL suspension. Data are mean ± SD (n = 3).

due to its high negative charge, which might prevent RBCs (−15 mV)[44] from interacting at further increased nanoparticle concentration. For mesoporous SiO_2 of all geometries tested, no hemolytic toxicity was observed below 100 μg/mL. The impact of nanoparticle geometry became pronounced as the concentration further increased. Mesoporous SiO_2 with high aspect ratio demonstrated lower hemolytic activity than spherical or low aspect ratio mesoporous SiO_2. It has been reported that the external surface area and the curvature of SiO_2 influence their hemolytic activity by affecting the magnitude of binding energy of particles with RBCs or bending energy of the membrane to wrap around the nanoparticles.[37] Large external surface area and small curvature (*i.e.*, $1/r^2$ for spheres) rendered the hemolysis process thermodynamically favorable.[37] In this case, the external surface areas of Stöber and Meso S were 24 and 109 m^2/g, respectively, which agreed well with previous similar calculations,[37,43] and had similar curvature due to the similar size they possessed. However, Meso S did not lead to a higher hemolytic rate than Stöber until the mass concentration exceeded beyond *ca.* 190 μg/mL. This indicates that there could possibly be a threshold in the density of silanol groups on each nanoparticle only above which it could cause immediate cell membrane damage upon exposure. Hence, the hemolytic activity depends not only on external surface area and curvature but also on silanol density of each nanoparticle exposed to RBCs.

The hemolytic activity of amine-modified SiO_2 was surface charge- and concentration-dependent (Figure 8). As the concentration increased, there was a rapid onset of hemolysis for all types of nanoparticles. SA led to the lowest extent of hemolysis possibly because of its lowest surface charge, whereas amine-modified mesoporous SiO_2 caused similar rates of hemolysis. The concentrations of SiO_2 leading to 10% hemolysis (LC_{10}) are summarized in Table 5. Zhao *et al.*[37] revealed that the affinity of SiO_2 to RBCs decreased with increasing degree of surface functionality independent of surface charge (−43 to 7 mV). Results from our study as shown in Table 5 suggest that increasing the surface charge beyond a certain threshold (>30 mV) might lead to an opposite effect including enhanced interaction of nanoparticles with RBCs and the resultant elevated hemolysis by amine-modified mesoporous

TABLE 5. Summary of LC_{10} Values of SiO_2 in Human Erythrocytes[a]

	LC_{10} values (μg/mL)				
	Stöber	Meso S	AR2	AR4	AR8
bare nanoparticles[b]	36 ± 1	154 ± 4	115 ± 1	152 ± 2	302 ± 3
amine-modified nanoparticles	97 ± 4	30 ± 1	40 ± 1	23 ± 1	43 ± 1

[a] Data are mean ± SD ($n = 3$). [b] There was a significant difference between the LC_{10} value of bare SiO_2 and that of amine-modified counterparts ($p < 0.001$).

SiO_2, in agreement with the cellular association results (Figure 6A,B). It must be noted that a good correlation with results of different experiments is based on a similar dose (*ca.* ≤ 100 μg/mL SiO_2). As the dose changes beyond a certain range, the pattern from different experiments shifts, and the correlation of various experiments at that dosage needs to be further validated.

CONCLUSION

In summary, nonporous Stöber silica nanospheres, mesoporous silica nanospheres, mesoporous silica nanorods with aspect ratios of 2, 4, and 8, and their cationic charged counterparts were synthesized and characterized. The porosity, shape, and surface modification effects on cellular toxicity or hemolytic activity were evaluated on macrophages, cancer epithelial cells, and human erythrocytes. The toxicity of SiO_2 was found to be cell-type-dependent. Cancer epithelial cells were highly resistant to nanoparticle treatment, while the toxicity on macrophages was predominantly surface-charge-dependent. The difference in toxicity between the two cell types could be due to the difference in the physiological function of each. Porosity and surface characteristics of the nanoparticles were the major factors that influenced the cellular association of the nanoparticles. Geometry did not seem to influence the extent of cellular association of the nanoparticles either at the early time point or over extended duration. Initial comparison of blood biocompatibility of nonporous and mesoporous SiO_2 with varied shapes and surface characteristics has been demonstrated using the hemolysis assay. Bare SiO_2 showed a porosity- and geometry-dependent hemolytic activity on RBCs with mesoporous SiO_2 at high aspect ratio exhibiting a reduced hemolytic activity. The extent of hemolysis was highly zeta-potential-dependent among the amine-modified SiO_2, and results indicated that there could be a surface charge "threshold" below which the amine modification on SiO_2 could lead to reduced hemolysis compared with their bare counterparts. Further studies evaluating the *in vivo* toxicity of SiO_2 in animal models are needed to establish an *in vitro*–*in vivo* correlation for better prediction of toxicity in biological systems.

METHODS

Synthesis of Nonporous and Mesoporous SiO_2. Nonporous silica nanoparticles (Stöber) were produced using the modified Stöber method.[23] Water (34.82 mL), 3.25 mL of ammonium hydroxide (29.7%), and 100 mL of ethanol were mixed and stabilized at 40 °C. Tetraethyl orthosilicate (6.20 mL) was added at an injection rate of 5 mL/min upon stirring at 550 rpm. The reaction was conducted for 1 h, and the product was washed twice by ethanol and stored in ethanol. Mesoporous SiO_2 of different shapes were synthesized through a one-step condensation under dilute silica source and low surfactant concentration conditions with ammonium hydroxide as the base catalyst.[24–29] Generally, cetyltrimethylammonium bromide was dissolved in aqueous medium with mild heating (30 °C). After the solution was cooled to room temperature (22 °C), aqueous ammonia was introduced and the mixture was stirred for an hour. TEOS was added at the rate of 5 mL/min while the stirring continued. The mixture was further stirred for 4 h, and the product was autoclaved at 100 °C for 24 h.[30,31] Subsequently the product was collected by centrifugation at 15 000 rpm for 20 min. As-synthesized nanoparticles were suspended in ethanolic HCl (1.5 mL of HCl in 150 mL of ethanol) and heated at 60 °C for 6 h to remove the surfactant. The complete removal of CTAB was confirmed by Fourier transform infrared (FT-IR) spectroscopy.

Surface Functionalization. To modify the surface of SiO_2 with primary amine functionalities,[33] 100 mg of SiO_2 was resuspended in 100 mL of anhydrous ethanol. (3-Aminopropyl-)triethoxysilane (APTES) was introduced dropwise to the SiO_2 suspension upon stirring at 500 rpm under nitrogen flow. The mixture was stirred at room temperature for 20 h. Amine-modified SiO_2 were collected by centrifugation and washed extensively with ethanol and water. SiO_2 were stored in ethanol at 4 °C and transferred to water immediately before use.

Nanoparticle Characterization. Transmission electron microscopy images were taken with a Philips Tecnai microscope operating at 120 kV. FT-IR spectra were recorded on a Varian Cary FT-IR 1000 spectrometer using KBr pellets. X-ray diffraction patterns of SiO_2 were analyzed on a Philips PANalytical X'Pert X-ray diffractometer (Spectris, England) using Cu Ka radiation (λ = 0.1542 nm) at 45 kV and 40 mA. The XRD spectra were recorded in the 2θ range of 2–10 with a step size of 0.02° in a 2θ scattering angle and a scanning speed of 0.01 deg/s. The slit sizes and specimen length were also adjusted for divergence slit, antiscattered slit, and receiving slit to suit the low-angle detection. Nitrogen adsorption–desorption isotherm measurements were completed on a Micromeritics ASAP 2010 (Norcross, GA) accelerated surface area analyzer at −196 °C. The SiO_2 were dried at 100 °C overnight before analysis. The Brunauer–Emmett–Teller specific surface areas were calculated by using adsorption data at P/P_0 = 0.05–0.20.[19,21] The external surface areas of mesoporous SiO_2 were calculated from the *t* plots of their N_2 adsorption isotherms.[32] Pore volume and pore size distributions were obtained from an adsorption branch by using the Barrett, Joyner, and Halenda method.[19,21]

Acute Cytotoxicity Assay. The acute toxicity effect of SiO_2 was determined by the WST-8 assay on A549 cells or RAW 264.7 macrophages (ATCC, Manassas, VA). Cells from passages 5 through 20 were used with medium changing once every three days. A549 cells or RAW 264.7 macrophages were seeded at 8000 cells/well or 16 000 cells/well in a 96-well plate in F-12k medium or DMEM supplemented with 10% FBS and maintained in a humidified incubator for 24 h. SiO_2 at incremental concentration of 100, 250, or 500 μg/mL were added to cells. Supernatants

from nanoparticle stock solutions and respective growth medium served as controls. Post 24 h, old medium was aspirated, and cells were washed three times with PBS. A 100 μL amount of complete medium containing 10% (v/v) Cell Counting Kit-8 (Dojindo, Rockville, MD) was added to each well and incubated with cells for 2 h. The absorbance of the plate was recorded at 450 nm on a UV/vis reader with a reference wavelength of 650 nm.

Proliferation Inhibition Assay. The cytotoxicity of SiO_2 was evaluated by the WST-8 viability assay on A549 cells or RAW264.7 macrophages. Initially, A549 or RAW cells were seeded at 2000 or 4000 cells/well in a 96-well plate and allowed to settle for 24 h. Then 10, 50, 100, 250, 500, or 1000 μg/mL of bare SiO_2 or amine-modified SiO_2 was added into the 96-well plate in triplicates. Supernatants from nanoparticle stock solutions and respective growth medium served as controls. Post 72 h, old medium was aspirated, and the following steps were the same as the procedures for the acute cytotoxicity assay described above.

Plasma Membrane Integrity Assay. Determination of propidium iodide uptake was used to assess the integrity of the plasma membrane of nanoparticle-dosed cells. A549 cells or RAW cells were seeded at 8×10^4 or 1.6×10^5 cells/well on a 12-well plate in triplicate. After 24 h, selected nanoparticles were added into each well at the concentration of 250 μg/mL. Twenty-four hours later, cells and medium from each well were collected into a 5 mL flow cytometry tube. The cell suspension was centrifuged at 1000 rpm for 5 min, the supernatant was decanted, and the cells were resuspended in 100 μL of PBS. A 5 μL portion of propidium iodide solution (50 μg/mL in water) was added to each tube. The tube was gently vortexed and incubated for 15 min at room temperature in the dark. Then 400 μL of PBS was added into each tube, and the samples were analyzed by flow cytometry (FACScan analyzer, Becton Dickinson, Franklin Lakes, NJ) within an hour.

Quantitation of Cellular Association. Cellular association of SiO_2 was evaluated on A549 and RAW264.7 cells. A549 or RAW cells were seeded at 8×10^4 or 1.6×10^5 cells/well on a 12-well plate in triplicate, 24 h before the addition of particles. Cells were incubated with 100 μg/mL of SiO_2 for 24 h (37 °C, 5% CO_2). After cell/particle incubation, the old medium was aspirated and the cells were washed three times with PBS. Then the cells were treated with 0.5 mL of 0.1% (v/v) Triton X-100 solution in water for 15 min. After that, the cell lysate was collected into a centrifuge tube, and the wells were further washed with 0.5 mL of water. The wash was also collected into the same centrifuge tube. Aliquots of 100 μL of cell lysate were used for protein content measurement by BCA assay (Thermo Scientific, Rockford, IL). The concentration of silicon in the cell lysate was measured by direct Si measurement using inductively coupled plasma mass spectrometry (Agilent 7500, Agilent Technologies, Santa Clara, CA). The amount of cellular-associated SiO_2 post 1 h incubation at 4 or 37 °C was also measured. RAW cells were seeded at 3.2×10^5 cells/well on a 12-well plate in triplicate and incubated for 24 h. After that, cells were preconditioned to 4 °C by incubating at 4 °C for a brief period of 10 min. Then silica nanoparticles were added to the cells at a concentration of 100 μg/mL, and the cells were further incubated at 4 °C for another hour. The treatment that followed was the same as mentioned above. To make sure that relative cell viability in the 4 °C treated plate was not dramatically influenced by exposure to cold temperature for the experimental duration, the relative viability from the 4 °C treated plate was compared with cells incubated at 37 °C for 70 min by the WST-8 assay.

Hemolysis. Heparin-stabilized human blood was freshly collected according to an approved University of Utah Institutional Review Board protocol and used within 3 h of being drawn.[36,43] A 4 mL sample of whole blood was added to 8 mL of Dulbecco's phosphate-buffered saline (D-PBS), and the RBCs were isolated from serum by centrifugation at 10016*g* for 5 min. The RBCs were further washed five times with sterile D-PBS solution. Following the last wash, the RBCs were diluted to 40 mL of D-PBS. Then 0.2 mL of the diluted RBC suspension was added to 0.8 mL of the silica nanoparticle suspension in D-PBS at a concentration of 12.5, 62.5, 125, 312.5, or 625 μg/mL to make the final nanoparticle concentration 10, 50, 100, 250, or 500 μg/mL. All samples were prepared in triplicate, and the suspension was briefly vortexed before leaving at static conditions at room temperature for 4 h. After that, the mixture was briefly vortexed again and centrifuged at 10016*g* for 3 min. A 100 μL amount of supernatant from the sample tube was transferred to a 96-well plate. The absorbance value of hemoglobin at 577 nm was measured with the reference wavelength of 655 nm. A 0.2 mL amount of diluted RBC suspension incubated with 0.8 mL of D-PBS and 0.8 mL of water was used as the negative or positive control. The percent of hemolysis was calculated as follows: Hemolysis % = [(sample absorbance − negative control)/(positive control − negative control)] × 100%.

Statistical Analysis. The difference between multiple groups was analyzed by one-way ANOVA. The Tukey post test was used where a difference was detected. For two-group comparison, Student's *t*-test was used. The difference between two groups was considered significant when $p < 0.05$. The LC_{10} values in the hemolysis assay were determined by using ED50plus v1.0 software.

Acknowledgment. We would like to acknowledge Dr. Sajo Naik (Western Research Institute, Cheyenne, WY) for his technical suggestions for mesoporous silica nanoparticle synthesis, and Dr. Khaled Greish for assistance with human blood withdrawal from lab volunteers. Financial support was provided by NIH grant R01 DE19050 and the Utah Science and Technology Research (USTAR) Initiative.

Supporting Information Available: Supplemental Calculation 1 and Supplemental Figures 1−5 are available free of charge *via* the Internet at http://pubs.acs.org.

REFERENCES AND NOTES

1. Barbé, C.; Bartlett, J.; Kong, L.; Finnie, K.; Lin, H.; Larkin, M.; Calleja, S.; Bush, A.; Calleja, G. Silica Particles: A Novel Drug-Delivery System. *Adv. Mater.* **2004**, *16*, 1–8.
2. Liong, M.; Lu, J.; Kovochich, M.; Xia, T.; Ruehm, S. G.; Nel, A. E.; Tamanoi, F.; Zink, J. I. Multifunctional Inorganic Nanoparticles for Imaging, Targeting, and Drug Delivery. *ACS Nano* **2008**, *2*, 889–896.
3. Vivero-Escoto, J. L.; Slowing, I. I.; Trewyn, B. G.; Lin, V. S. Mesoporous Silica Nanoparticles for Intracellular Controlled Drug Delivery. *Small* **2010**, *6*, 1952–1967.
4. Lu, J.; Liong, M.; Li, Z.; Zink, J. I.; Tamanoi, F. Biocompatibility, Biodistribution, and Drug-Delivery Efficiency of Mesoporous Silica Nanoparticles for Cancer Therapy in Animals. *Small* **2010**, *6*, 1794–1805.
5. Li, L.; Tang, F.; Liu, H.; Liu, T.; Hao, N.; Chen, D.; Teng, X.; He, J. *In Vivo* Delivery of Silica Nanorattle Encapsulated Docetaxel for Liver Cancer Therapy with Low Toxicity and High Efficacy. *ACS Nano* **2010**, *4*, 6874–6882.
6. Tsai, C.-P.; Chen, C.-Y.; Hung, Y.; Chang, F.-H.; Mou, C.-Y. Monoclonal Antibody-Functionalized Mesoporous Silica Nanoparticles (MSN) for Selective Targeting Breast Cancer Cells. *J. Mater. Chem.* **2009**, *19*, 5737–5743.
7. Cheng, S.-H.; Lee, C.-H.; Chen, M.-C.; Souris, J. S.; Tseng, F.-G.; Yang, C.-S.; Mou, C.-Y.; Chen, C.-T.; Lo, L.-W. Tri-Functionalization of Mesoporous Silica Nanoparticles for Comprehensive Cancer Theranostics-the Trio of Imaging, Targeting and Therapy. *J. Mater. Chem.* **2010**, *20*, 6149–6157.
8. Nan, A.; Bai, X.; Son, S. J.; Lee, S. B.; Ghandehari, H. Cellular Uptake and Cytotoxicity of Silica Nanotubes. *Nano Lett.* **2008**, *8*, 2150–2154.
9. Son, S. J.; Bai, X.; Nan, A.; Ghandehari, H.; Lee, S. B. Template Synthesis of Multifunctional Nanotubes for Controlled Release. *J. Controlled Release* **2006**, *114*, 143–152.
10. Chen, C.-C.; Liu, Y.-C.; Wu, C.-H.; Yeh, C.-C.; Su, M.-T.; Wu, Y.-C. Preparation of Fluorescent Silica Nanotubes and Their Application in Gene Delivery. *Adv. Mater.* **2005**, *17*, 404–407.
11. Buyukserin, F.; Medley, C. D.; Mota, M. O.; Kececi, K.; Rogers, R. R.; Tan, W.; Martin, C. R. Antibody-Functionalized Nano

Test Tubes Target Breast Cancer Cells. *Nanomedicine (London)* **2008**, *3*, 283–292.
12. Hudson, S. P.; Padera, R. F.; Langer, R.; Kohane, D. S. The Biocompatibility of Mesoporous Silicates. *Biomaterials* **2008**, *29*, 4045–4055.
13. Gratton, S. E.; Ropp, P. A.; Pohlhaus, P. D.; Luft, J. C.; Madden, V. J.; Napier, M. E.; DeSimone, J. M. The Effect of Particle Design on Cellular Internalization Pathways. *Proc. Natl. Acad. Sci. U. S. A.* **2008**, *105*, 11613–11618.
14. Muro, S.; Garnacho, C.; Champion, J. A.; Leferovich, J.; Gajewski, C.; Schuchman, E. H.; Mitragotri, S.; Muzykantov, V. R. Control of Endothelial Targeting and Intracellular Delivery of Therapeutic Enzymes by Modulating the Size and Shape of ICAM-1-Targeted Carriers. *Mol. Ther.* **2008**, *16*, 1450–1458.
15. Arnida; Janat-Amsbury, M. M.; Ray, A.; Peterson, C. M.; Ghandehari, H. Geometry and Surface Characteristics of Gold Nanoparticles Influence Their Biodistribution and Uptake by Macrophages. *Eur. J. Pharm. Biopharm.* **2011**, *77*, 417–423.
16. Nguyen, T. P. B.; Lee, J.-W.; Shim, W. G.; Moon, H. Synthesis of Functionalized SBA-15 with Ordered Large Pore Size and Its Adsorption Properties of BSA. *Microporous Mesoporous Mater.* **2008**, *110*, 560–569.
17. Maurer-Jones, M. A.; Lin, Y. S.; Haynes, C. L. Functional Assessment of Metal Oxide Nanoparticle Toxicity in Immune Cells. *ACS Nano* **2010**, *4*, 3363–3373.
18. Slowing, I.; Trewyn, B. G.; Lin, V. S. Effect of Surface Functionalization of MCM-41-Type Mesoporous Silica Nanoparticles on the Endocytosis by Human Cancer Cells. *J. Am. Chem. Soc.* **2006**, *128*, 14792–14793.
19. Lu, F.; Wu, S. H.; Hung, Y.; Mou, C. Y. Size Effect on Cell Uptake in Well-Suspended, Uniform Mesoporous Silica Nanoparticles. *Small* **2009**, *5*, 1408–1413.
20. He, Q.; Zhang, Z.; Gao, Y.; Shi, J.; Li, Y. Intracellular Localization and Cytotoxicity of Spherical Mesoporous Silica Nano- and Microparticles. *Small* **2009**, *5*, 2722–2729.
21. Tsai, C. P.; Hung, Y.; Chou, Y. H.; Huang, D. M.; Hsiao, J. K.; Chang, C.; Chen, Y. C.; Mou, C. Y. High-Contrast Paramagnetic Fluorescent Mesoporous Silica Nanorods as a Multifunctional Cell-Imaging Probe. *Small* **2008**, *4*, 186–191.
22. Dobrovolskaia, M. A.; Aggarwal, P.; Hall, J. B.; McNeil, S. E. Preclinical Studies to Understand Nanoparticle Interaction with the Immune System and Its Potential Effects on Nanoparticle Biodistribution. *Mol. Pharm.* **2008**, *5*, 487–495.
23. Chung, Y. S.; Jeon, M. Y.; Kim, C. K. Fabrication of Nearly Monodispersed Silica Nanoparticles by Using Poly(1-Vinyl-2-Pyrrollidinone) and Their Application to the Preparation of Nanocomposites. *Macromol. Res.* **2009**, *17*, 37–43.
24. Giri, S.; Trewyn, B. G.; Stellmaker, M. P.; Lin, V. S.-Y. Stimuli-Responsive Controlled-Release Delivery System Based on Mesoporous Silica Nanorods Capped with Magnetic Nanoparticles. *Angew. Chem., Int. Ed.* **2005**, *44*, 5038–5044.
25. Huh, S.; Wiench, J. W.; Yoo, J.-C.; Pruski, M.; Lin, V. S.-Y. Organic Functionalization and Morphology Control of Mesoporous Silicas Via a Co-Condensation Synthesis Method. *Chem. Mater.* **2003**, *15*, 4247–4256.
26. Naik, S. P.; Elangovan, S. P.; Okubo, T.; Sokolov, I. Morphology Control of Mesoporous Silica Particles. *J. Phys. Chem. C* **2007**, *111*, 11168–11173.
27. Yang, S.; Zhao, L.; Yu, C.; Zhou, X.; Tang, J.; Yuan, P.; Chen, D.; Zhao, D. On the Origin of Helical Mesostructures. *J. Am. Chem. Soc.* **2006**, *128*, 10460–10466.
28. Lelong, G.; Bhattacharyya, S.; Kline, S.; Cacciaguerra, T.; Gonzalez, M. A.; Saboungi, M.-L. Effect of Surfactant Concentration on the Morphology and Texture of MCM-41 Materials. *J. Phys. Chem. C* **2008**, *112*, 10674–10680.
29. Jin, H.; Liu, Z.; Ohsuna, T.; Terasaki, O.; Inoue, Y.; Sakamoto, K.; Nakanishi, T.; Ariga, K.; Che, S. Control of Morphology and Helicity of Chiral Mesoporous Silica. *Adv. Mater.* **2006**, *18*, 593–596.
30. Kim, J. M.; Kwak, J. H.; Jun, S.; Ryoo, R. Ion Exchange and Thermal Stability of MCM-41. *J. Phys. Chem.* **1995**, *99*, 16742–16747.
31. Ryoo, R.; Jun, S. Improvement of Hydrothermal Stability of MCM-41 Using Salt Effects During the Crystallization Process. *J. Phys. Chem. B* **1997**, *101*, 317–320.
32. Zhu, H. Y.; Zhao, X. S.; Liu, G. Q.; Do, D. D. Improved Comparison Plot Method for Pore Structrue Characterizatoin of MCM-41. *Langmuir* **1996**, *12*, 6513–6517.
33. Kobler, J.; Moller, K.; Bein, T. Colloidal Suspensions of Functionalized Mesoporous Silica Nanoparticles. *ACS Nano* **2008**, *2*, 791–799.
34. Jones, C. F.; Grainger, D. W. *In Vitro* Assessments of Nanomaterial Toxicity. *Adv. Drug Delivery Rev.* **2009**, *61*, 438–456.
35. Riccardi, C.; Nicoletti, I. Analysis of Apoptosis by Propidium Iodide Staining and Flow Cytometry. *Nat. Protoc.* **2006**, *1*, 1458–1461.
36. Slowing, I. I.; Wu, C. W.; Vivero-Escoto, J. L.; Lin, V. S. Mesoporous Silica Nanoparticles for Reducing Hemolytic Activity Towards Mammalian Red Blood Cells. *Small* **2009**, *5*, 57–62.
37. Zhao, Y.; Sun, X.; Zhang, G.; Trewyn, B. G.; Slowing, I. I.; Lin, V. S. Interaction of Mesoporous Silica Nanoparticles with Human Red Blood Cell Membranes: Size and Surface Effects. *ACS Nano* **2011**, *5*, 1366–1375.
38. Xing, X.; He, X.; Peng, J.; Wang, K.; Tan, W. Uptake of Silica-Coated Nanoparticles by Hela Cells. *J. Nanosci. Nanotechnol.* **2005**, *5*, 1688–1693.
39. Tao, Z.; Toms, B. B.; Goodisman, J.; Asefa, T. Mesoporosity and Functional Group Dependent Endocytosis and Cytotoxicity of Silica Nanomaterials. *Chem. Res. Toxicol.* **2009**, *22*, 1869–1880.
40. Petushkov, A.; Intra, J.; Graham, J. B.; Larsen, S. C.; Salem, A. K. Effect of Crystal Size and Surface Functionalization on the Cytotoxicity of Silicalite-1 Nanoparticles. *Chem. Res. Toxicol.* **2009**, *22*, 1359–1368.
41. Chung, T. H.; Wu, S. H.; Yao, M.; Lu, C. W.; Lin, Y. S.; Hung, Y.; Mou, C. Y.; Chen, Y. C.; Huang, D. M. The Effect of Surface Charge on the Uptake and Biological Function of Mesoporous Silica Nanoparticles in 3t3-L1 Cells and Human Mesenchymal Stem Cells. *Biomaterials* **2007**, *28*, 2959–2966.
42. Nabeshi, H.; Yoshikawa, T.; Arimori, A.; Yoshida, T.; Tochigi, S.; Hirai, T.; Akase, T.; Nagano, K.; Abe, Y.; Kamada, H.; *et al.* Effect of Surface Properties of Silica Nanoparticles on Their Cytotoxicity and Cellular Distribution in Murine Macrophages. *Nanoscale Res. Lett.* **2011**, *6*, 1–6.
43. Lin, Y. S.; Haynes, C. L. Impacts of Mesoporous Silica Nanoparticle Size, Pore Ordering, and Pore Integrity on Hemolytic Activity. *J. Am. Chem. Soc.* **2010**, *132*, 4834–4842.
44. Jan, K. M.; Chien, S. Role of Surface Electric Charge in Red Blood Cell Interactions. *J. Gen. Physiol.* **1973**, *61*, 638–654.